UNIVERSITÀ DEGLI STUDI DI PADOVA

DIPARTIMENTO DI BIOLOGIA

Corso di Laurea magistrale in Molecular Biology

TESI DI LAUREA

Targeting mitochondrial calcium transfer to treat amyotrophic lateral sclerosis using the novel photoconvertible ratiometric Ca^{2+} sensor CaMPARI

Relatore: Prof. Luigi Leanza
Dipartimento di Biologia

Correlatore: Prof. Nicolas Demaurex
Université de Genève, Centre Médicale Universitaire, Département de Physiologie Cellulaire et Métabolisme

Laureando: Benjamin James Seiple

ANNO ACCADEMICO 2022/2023

Abstract

Intracellular membrane contact sites facilitate the transfer of ions, metabolites, and other molecules between subcellular compartments. Mitochondrial-associated membranes (MAMs) of the ER are particularly important for regulating the metabolic and energetic equilibria of the cell, and dysfunctions in MAMs are implicated in many pathologies. One of the most important roles of the MAMs and an indicator of their functionality is the transfer of Ca^{2+} from the ER to the mitochondrion. However, measuring Ca^{2+} levels in subcellular compartments, despite the existence of many high fidelity, targetable dyes and indicators, is still limited to single-cell observations and not conducive to studying populations of cells. To address this limitation, a genetically encoded calcium indicator (GECI) called CaMPARI (Calmodulin modulatable photoactivatable ratiometric indicator) was characterized as an effective means of measuring intracellular Ca^{2+} in cell populations. CaMPARI was then used to measure intracellular both evoked and basal Ca^{2+} transfer dynamics in HEK293T, HeLa, and NSC34 cells differentially expressing the MAMs resident protein IP3R1 to model the Ca^{2+} dynamics of MAMs disturbance.

Introduction

MAMs Stucture & Function

Mitochondrial Associated Membranes (MAMs) are dynamic organelle contact sites between the Endoplasmic Reticulum (ER) and the mitochondria that act as subcellular signaling hubs in response to the various physiological conditions of the cell (1). Thus far, MAMs have been implicated in the regulation of numerous cellular processes, primarily in lipid transfer and intracellular Ca^{2+} signaling, but also in redox control, inflammasome formation, mitochondrial bioenergetics, autophagy, and cell death (1, 2, 3). The physical structure of the MAMs has been elucidated primarily through electron microscopy (EM) as they compose approximately 5-20% of the mitochondrial surface area and ~10-50 nm distance between the ER and the mitochondria. However, while EM has remained the gold standard for the imaging of MAMs, live-cell imaging has proven itself invaluable for functional analysis (4). Additionally, MAMs have a high degree of structural and compositional heterogeneity with a large diversity of functional proteins and protein linkers localized to them (5). Despite this heterogeneity, there is a subset of these proteins that is consistently found in the MAMs contributing to their core functions. These include ER and mitochondrial ion channels like the inositol 1,4,5 triphosphate receptor (IP3R) and the voltage dependent anion channel 1 (VDAC1), chaperones like 75kDa-glucose regulated protein (GRP75), inflammasome components like thioredoxin-interacting protein (TXNIP), lipid synthesis and transfer proteins such as serine active site containing 1 (SERAC1), and mitochondrial shaping proteins like mitofusins 1 and 2 (MFN1 and MFN2) (1).

Ca^{2+} Signaling in the MAMs

The ER acts as an intracellular Ca^{2+} store designed to sequester Ca^{2+} and keep Ca^{2+} concentration in the cytoplasm low and available for mobilization at a moment's notice. In order to maintain this balance, the ER uses a variety of intruding and extruding

mechanisms including Sarco-Endoplasmic Reticulum Calcium ATPase (SERCA), which expends ATP to pump Ca^{2+} inside the ER, and ion channels in the ER like the Ryanodine Receptor or IP3R which allow Ca^{2+} to exit the ER down its concentration gradient (6). In addition to releasing Ca^{2+} directly into the cytoplasm, the ER forms membrane contact sites (MCS) with various other organelles, allowing the release of Ca^{2+} into these MCS and thus into the neighboring organelles. This occurs through the creation of a microdomain within the MCS where the local Ca^{2+} concentration is much higher than the concentration resulting from cytosolic Ca^{2+} diffusion after release from the ER. The MAMs' role as one of these MCS is inextricably linked to the transfer of Ca^{2+} from the intracellular stores in the ER to the mitochondrial matrix and its modulation by other cellular processes and signals (7).

Ca^{2+} transfer at the MAMs is regulated by extra and intracellular signals transducible through the protein components populating the MAMs. MAMs Ca^{2+} transfer was first observed as large spikes in Ca^{2+} concentration evoked by an agonist (8). Canonically, an extracellular signal such as a Ca^{2+}-mobilizing agonist binds a G-Protein Coupled Receptor (GPCR) on the plasma membrane (PM), activating Phospholipase C (PLC), which in turn to production of Inositol-1,4,5-triphosphate (IP_3) from the hydrolysis of Phosphatidylinositol-4,5-bisphosphate (PIP_2), which diffuses through the cytoplasm to the MAMs where it binds to the cytosolic face of IP3R1, IP3R2, and IP3R3 at the ER membrane (9). IP3Rs are homo or heterotrimeric ligand-gated Ca^{2+} channels which, upon opening, create a microdomain of Ca^{2+} in the MAMs space. They are also responsive to cytosolic Ca^{2+} which inhibits IP3R at high concentrations, adding an additional level of regulation (10). The Ca^{2+} microdomains produced by the opening of IP3R promote the flow of Ca^{2+} into the mitochondria through the Voltage Dependent Anion Channels (VDAC) in the Outer Mitochondrial Membrane (OMM), which creates a high concentration of Ca^{2+} in the Intermembrane Space (IMS). The rate limiting step for the transfer of Ca^{2+} into the mitochondrial matrix is the low conductance of the Mitochondrial Ca^{2+} Uniporter (MCU) channel population in the Inner Mitochondrial Membrane (IMM). This rate limiting step is modulated by the increased concentration of Ca^{2+} in the IMS, which makes it possible for the MCU to conduct Ca^{2+} into the mitochondrial matrix (11, 12) (Fig. 1D)

There is also evidence that the transfer of Ca^{2+} across by means of the IP3R can occur as small spontaneous Ca^{2+} puffs rather than as a cohesive spike (13). However, given the fleeting and low magnitude nature of these puffs, their measurement has proved to be difficult thus far, possible only with Total Internal Reflection Fluorescence (TIRF) microscopy. TIRF microscopy permits high resolution imaging of membranes and MCS by directing light with a low angle of incidence towards the bottom of the coverslip where only the several hundred nanometers of the cell closest to the coverslip can be observed. Imaging cells as such increases the signal to noise ratio in the image and decreases the risk of fluorescent photobleaching, but provides an extremely narrow field of view (14). Through investigation of the three IP3R isoforms using TIRF microscopy, it was found

that each one has a unique activity pattern in relation to the production of Ca^{2+} puffs. The importance of these puffs still remains unclear, but there is an observable alteration in them upon modulation of the IP3Rs (13). Nonetheless, the measurability of these puffs has remained a challenge to in-depth study of them, their mechanics, and their potential functions. TIRF microscopy cannot measure the MAMs directly, and electrophysiology cannot measure them either, bringing into question whether Ca^{2+} puffs even occur at the MAMs. Thus, new, more precise techniques are needed to thoroughly investigate this phenomenon and its potential function in the MAMs.

Role of Ca^{2+} in Mitochondria

Once transferred to the mitochondrial matrix, Ca^{2+} can play a plethora of roles. It has been implicated in the remodeling of intracellular Ca^{2+} flux, as well as in the buffering of intracellular Ca^{2+} (15). Mitochondrial Ca^{2+} has also been shown to play a role in the regulation of ATP production (16), the NAD+/NADH balance in the cytosol (17), and the prevention of bioenergetic stress (18). In addition, an overload in mitochondrial Ca^{2+} concentration has been proposed as a mechanism in the formation of the mitochondrial Permeability Transition Pore (PTP) in the IMM, leading to increased mitochondrial permeability and extrusion of mitochondrial Electron Transport Chain (ETC) components. The final result is a mitochondrial regulation of apoptosis (19).

Modulation of MAMs in Human Disease

Given their expansive roles in maintenance of cellular homeostasis and signaling, the perturbation of the MAMs has been implicated in many human pathologies (20). From inflammation, to cancer (21), to neurological disorders, MAMs and MAMs-localized proteins are promising pharmaceutical targets for many diseases. VAPB-PTP1P5, for example, is one of the tethering structures present at the MAMs and is implicated in amyotrophic lateral sclerosis (ALS), a debilitating degenerative motor neuron disease. A VAPB mutant appears in many patients with the familial form of the disease, and it is implicated in the perturbation of MAMs Ca^{2+} dynamics (22). The MAMs' role in ALS is of particular interest, as several MAMs-targeted proteins in addition to VAPB have been found to be involved in the disease, but given the difficulty of studying the MAMs, their exact role has yet to be elucidated (23). One of the goals of this research is to improve our understanding of how to study MAMs in order to target diseases like ALS.

Existing Tools to study MAMs Ca^{2+} transfer

The most commonly used method for the measurement of Ca^{2+} flux anywhere in the cell is live-cell imaging microscopy with fluorescent probes, which provides high spatial and temporal resolution. A wide array of Ca^{2+}-sensitive dyes and Genetically Encoded Calcium Indicators (GECIs) are available to use in conjunction with live-cell imaging setups with various Ca^{2+} binding affinities, emission spectra, diffusibility, and targeting location. It is particularly essential that these GECIs are designed with an appropriate Ca^{2+} binding affinity for the subcellular compartment in question, as Ca^{2+} concentration can vary widely across different parts of the cell. In the cytoplasm or mitochondria, [Ca^{2+}]

generally lies around ~100 nm at rest, while in the ER [Ca^{2+}] can reach 500 uM, necessitating sensors with binding affinities (Kd) in those ranges in order to provide a sufficient dynamic range to react to fluctuations in [Ca^{2+}] (24). For example, R-mito-Geco is a red mitochondrial-targeted sensor with a Kd of ~150 nm, allowing measurement of Ca^{2+} in a dynamic range of ~100-1000 nm (25).

Despite the wide adaptability of live cell imaging, it is subject to several limitations. As with all microscopy, there is inherent human bias in the selection of cells to be analyzed. There is the added disadvantage in the often low-throughput nature of the data collected which, even with microscopes optimized for taking multiple measurements simultaneously, require extensive analysis. Additionally, live cell imaging requires lower illumination intensity and exposure time in order to avoid extreme perturbation of the cells being observed, decreasing the maximum reachable signal-to-noise ratio and losing subtle or low intensity fluorescent changes (26).

CaMPARI

CaMPARI (Calcium Modulated Photoactivatable Ratiometric Integrator) is a GECI with the unique ability to irreversibly alter its fluorescence upon simultaneous exposure to high cellular Ca^{2+} levels and 405 nm photoconverting (PC) light (27). Upon reception of a physiological Ca^{2+} stimulus in the range of CaMPARI's Kd of 110nM, its green fluorescence of ~520 nm will transiently decrease. However, when 405 nm PC light is applied to cells expressing CaMPARI, this Ca^{2+}-induced transient decrease becomes irreversible and is accompanied by a proportional increase in red fluorescence of ~580 nm. The mechanistic basis of these irreversible changes in fluorescence is guided by CaMPARI's design; it is made up of a Calmodulin (CaM)-based Ca^{2+}-sensing domain, the Ca^{2+}-sensing CaM-associated peptide M13, and a photoconvertible fluorescent protein called EosFP. Ca^{2+} binding alters the conformation of the EosFP molecule, putting it into a permissive state for irreversible photoconversion when exposed to the appropriate wavelength of light. (Fig. 1B) This allows an integration over a fixed period of PC light exposure with a simplified readout of red fluorescence to green fluorescence which theoretically corresponds to CaMPARI's Ca^{2+} exposure (27, 28).

CaMPARI-FACS Technique

For the purposes of observing mitochondrial Ca^{2+} changes, three copies 23-aa cytochrome oxidase 8 (COX8) presequence were fused to the N-terminus of CaMPARI to target it to the mitochondrial matrix to create a new probe called mCamp2 (mitochondrial CaMPARI2) (Fig. 1A). The irreversible nature of CaMPARI's photoconversion allowed us to use it in an unconventional manner; rather than observing fluorescence changes under a microscope to track Ca^{2+}, we measured the red to green (RFP/GFP) fluorescence ratio of CaMPARI in each cell using Fluorescence Activated Cell Sorting (FACS) after a specified duration of exposure to PC light. (Fig.

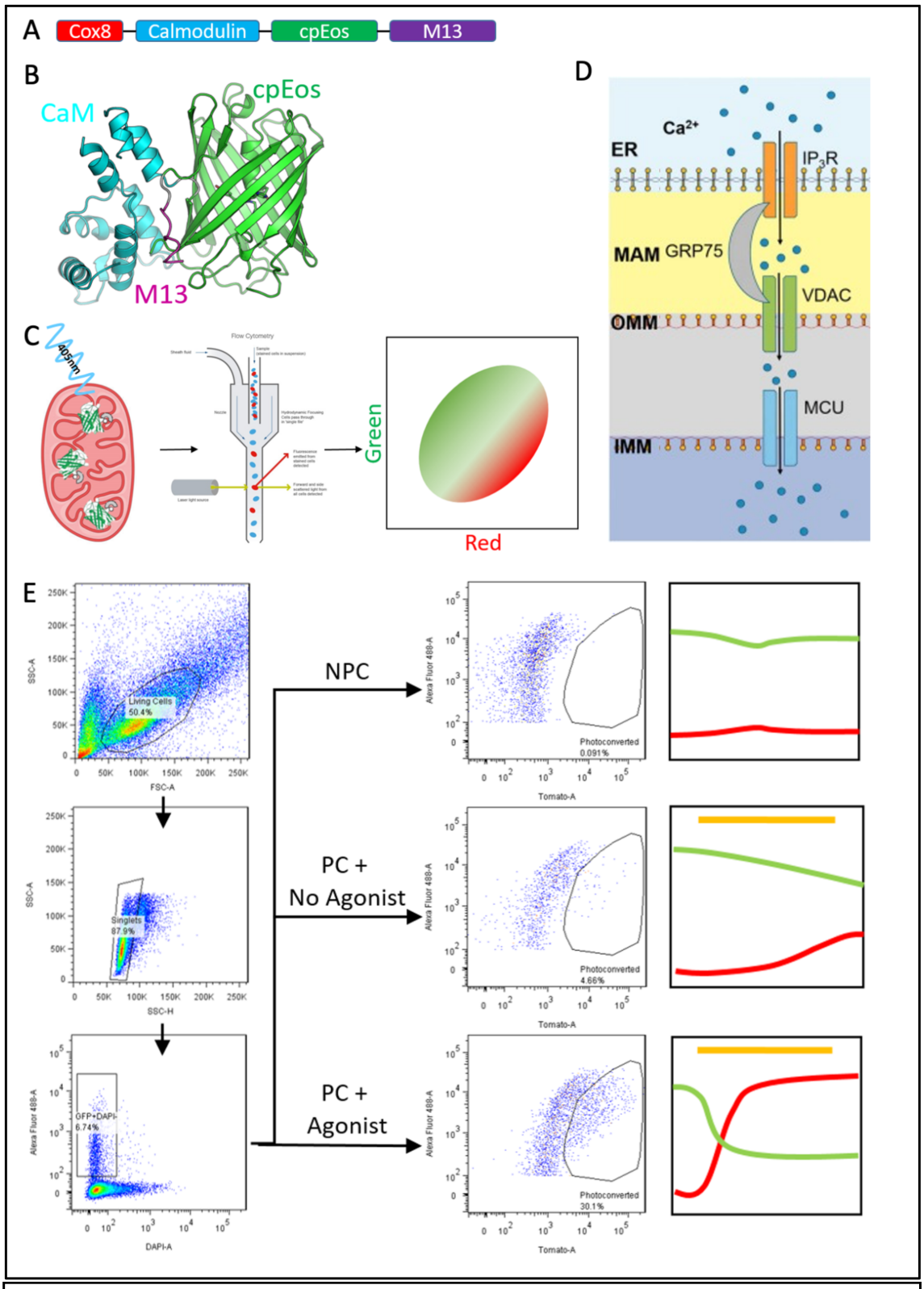

Figure 1. **Schematic representation of CaMPARI-FACS technique. A.** Primary structure of mCamp2. **B.** Crystal structure of cytosolic Camp2 taken from Fosque et al., 2015. **C.** Workflow of CaMPARI-FACS technique, starting from expression of mCamp2 in the mitochondria and photoconversion by 405 nm light, followed by FACS sorting (image from abcam) and analysis of red to green ratio of the cell population. **D**.

Cartoon illustrating the flow of Ca^{2+} across the MAMs and the machinery involved (adapted from 29). **E**. Gating of the FACS analysis began with isolation of living cells by shape, drilling down into singlets, then selection of living transfected cells (GFP+DAPI-). Cells were exposed to three conditions: NPC (non-photoconverted), PC (photoconverted) + No Agonist, and PC + Agonist. In the fourth column, the mCamp2 fluorescence in the GFP channel (green) and RFP channel (red) are shown in response to exposure to photoconverting light (yellow).

1C) The novelty of this technique required us to test the efficacy of the tool in measuring Ca^{2+} by validating the probe's Ca^{2+} sensitivity and comparing its performance to results generated by more traditional techniques. Given CaMPARI's high sensitivity and potential applicability to higher throughput experiments in conjunction with FACS, we also hypothesized that it would be an excellent tool for the measurement of Ca^{2+} puffs and basal Ca^{2+} levels in the mitochondria and across the MAMs. Given the lack of understanding of these phenomena, particularly where it relates to human diseases, it is essential to have efficient and precise methods to measure them.

Results

Development of the CaMPARI-FACS Technique

The mCamp2 photoconversion response observed using live-cell imaging microscopy was used as a baseline for the setup of the FACS experiments with three conditions to provide adequate controls. In the first condition, mCamp2's spontaneous conversion to red in the absence of PC light was measured by exposing cells neither to a Ca^{2+}-mobilizing agonist nor to PC light in the No Photoconversion (NPC) control. In the second condition, mCamp2's basal conversion to red was measured in the absence of a Ca^{2+}-mobilizing agonist and the presence of PC light (PC + No Agonist). The PC + No Agonist condition was intended to detect the basal Ca^{2+} levels in the mitochondria as well as spontaneous conversion of the CaMPARI molecule in the presence of PC light. In the third condition, cells were exposed to both a Ca^{2+}-mobilizing agonist and PC light, corresponding to a measurement of an evoked Ca^{2+} transfer to the mitochondria, which is the commonly used metric in regards to MAMs functionality in Ca^{2+} signaling (Fig. 1E).

Two metrics were obtained from the FACS experiments with which to validate the CaMPARI-FACS technique: RFP/GFP ratio and percentage photoconversion (PC). The RFP/GFP ratio was calculated by dividing the average red fluorescence by the average green fluorescence of each sample, with an increased RFP/GFP ratio indicating an increased mCamp2 photoconversion. Percentage PC was calculated by drawing a gate on the NPC controls which excluded >99% of measured cells, thus setting a threshold for PC light and Ca^{2+}-dependent mCamp2 photoconversion. The variability of samples required that the gate used for calculating percentage PC be adjusted for each day the experiment was performed as well as each cell line. (Fig. 1E)

Validation of CaMPARI2

Ca^{2+} transfer from the ER to the Mitochondria measured by mCamp2 is comparable to established live-cell imaging techniques

In order to validate that the RFP/GFP ratios obtained from the experiments using the CaMPARI-FACS technique were a valid method of measuring Ca^{2+}, we compared live-cell imaging traces with the RFP/GFP ratios obtained from mCamp2-transfected cells which had been photoconverted and sorted using FACS. Three cell lines were utilized to provide a diverse range of model systems for mCamp2's use: HEK293T, HeLa, and NSC34. For each cell line, live-cell imaging microscopy was used in conjunction with Ca^{2+}-sensitive probes for measurement of cytosolic (Fura-2) (Fig. 2A) and mitochondrial Ca^{2+} (R-mito-Geco) (Fig. 2B). Each cell line was then characterized by their ratios of mitochondrial to cytosolic Ca^{2+} transient maxima (Fig. 2C), with HEK293T and NSC34 cells presenting the strongest evoked Ca^{2+} responses in mitochondria.

The same experiment was then performed on cells transfected with mCamp2 and exposed to PC light for 3 minutes. The RFP/GFP ratio and percentage PC metrics generally followed the same trends, indicating that despite the different features of the sample data used to calculate them, they provided similar information about the MAMs Ca^{2+} transfer. Both metrics did vary considerably from day to day, which could be attributed to variation in cell confluency in culture, preparation of agonists and imaging media, as well as ambient light levels in the room where the mCamp2 photoconversion was performed.

According to both metrics, there was a consistent and statistically significant trend of the PC + No Agonist condition undergoing less photoconversion than the PC + Agonist condition in all three cell lines (all p-values <0.0387) (Fig. 2E).

Interestingly, a significant change in the RFP/GFP ratio and percentage PC metrics was also observed between the NPC and the PC + No Agonist conditions in all three conditions (all p-values <0.0440) (Fig. 2E). This difference can be attributed to either mCamp2's Ca^{2+} dependence or another Ca^{2+}-independent feature of mCamp2 triggered by the addition of PC light. Ca^{2+}-dependent mechanisms could include Ca^{2+} present in the mitochondrial matrix at basal levels or a MAMs-mediated transfer occurring without stimulation by an agonist. Alternatively, a Ca^{2+}-independent spontaneous photoconversion of the mCamp2 probe could occur due to inherent properties of the probe, autofluorescence, or other changes in the cellular environment that affect its activity (25).

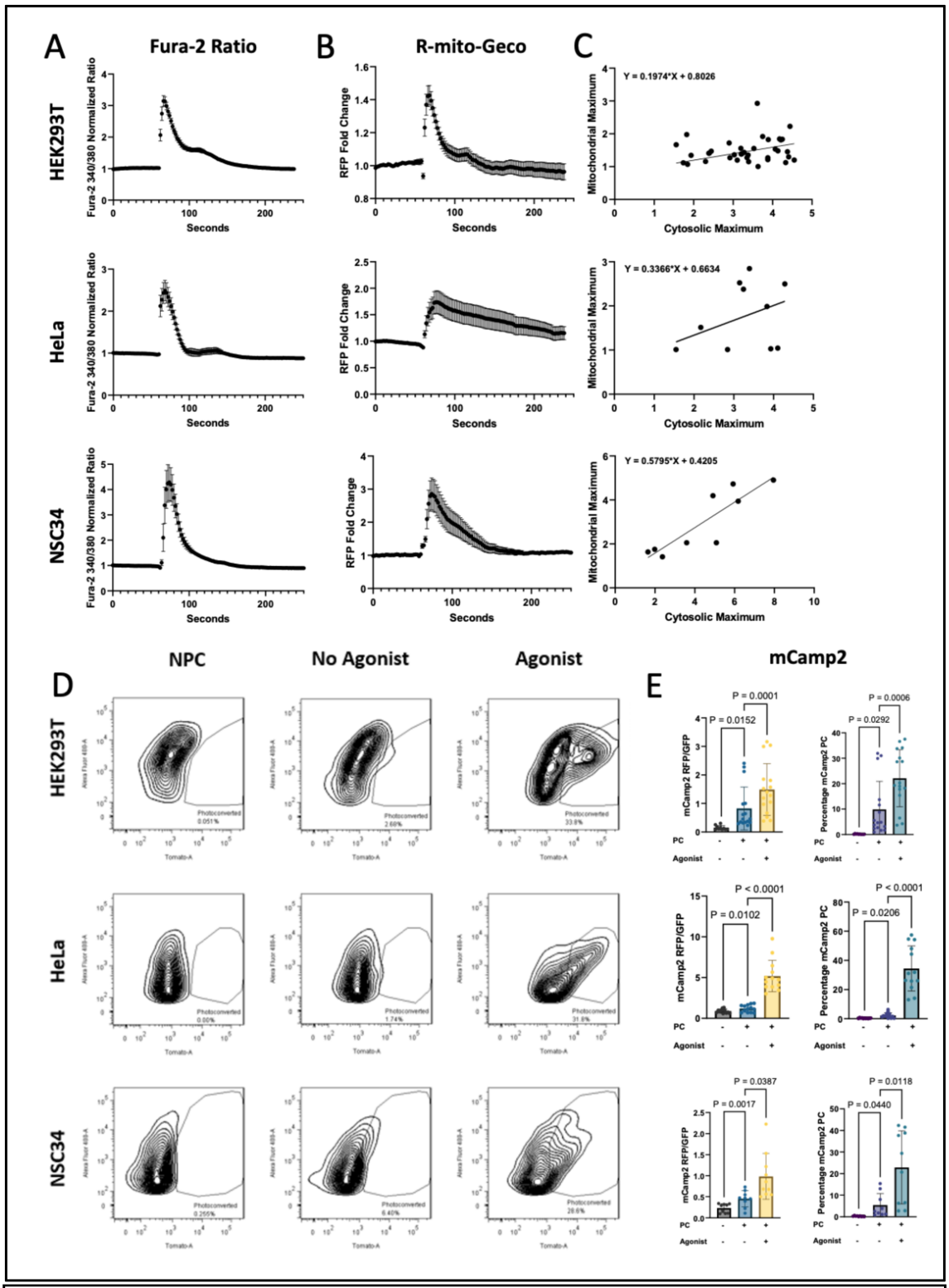

Figure 2. **The CaMPARI-FACS technique detects agonist-induced Ca^{2+} flux into the mitochondria. A.** HEK293T, HeLa, and NSC34 cells were stained with Fura-2 and cytosolic Ca^{2+} was imaged in live-cell microscopy in response to a Ca^{2+}-mobilizing agonist. For HEK293T and NSC34, 100uM ATP in Ca^{2+}-containing solution was used; for HeLa, 50uM Histamine in Ca^{2+}-containing solution was used. Traces were

normalized to the first 20 seconds of the recording. **B.** The mitochondrial Ca^{2+} transient was measured by transfected R-mito-GECO. Traces were normalized to the first 20 seconds of the recording. **C.** Cytoplasmic and mitochondrial transient maxima were calculated for each cell type and compared. Mitochondrial maxima on the y-axis and cytoplasmic maximum on the x-axis. **D**. FACS analysis completed using FlowJo for each of the three cell types show that cell populations undergo a shift towards a diagonal alignment and more red fluorescence upon exposure to PC light either in isolation or in combination with an agonist. Exposure to an agonist led to the largest red shift. **E.** Quantification of FACS samples were carried out for each cell type for both RFP/GFP Ratio and Percentage. HEK293T cells had n=16, HeLa had n=13, and NSC34 had n=10 for each condition, with each n representing one FACS tube containing at least 500 GFP+DAPI- cells. An ANOVA mixed-effects analysis with a Geisser-Greenhouse correction was done for each cell line, with significant differences observed between every condition in each cell line (all p-values <0.0440).

mCamp2 Measures Non-evoked Ca^{2+} Phenomena

In order to find the source of the basal activation in the PC + No Agonist condition observed in Fig. 2E, a mutagenized form of mCamp2 (mCamp2 Mutant) was used. The mCamp2 Mutant has a modified M13 loop incapable of undergoing its Ca^{2+}-induced conformational change, making it possible to distinguish between Ca^{2+}-dependent and Ca^{2+}-independent mCamp2 photoconversion (Fig. 3A). Using both live-cell imaging and FACS analysis, we compared the RFP/GFP ratio and percentage PC for cells transfected with mCamp2 Mutant in each condition with those of cells transfected with the functional mCamp2, hereon called mCamp2 WT. A large increase in red fluorescence was visually apparent with the addition of PC light and agonist for cells transfected with mCamp2 WT (Fig. 3B,D). However, when mCamp2 Mutant was used, only a marginal increase in the RFP/GFP ratio was observed even in the presence of PC light and a Ca^{2+}-mobilizing agonist, which was the condition which caused the highest degree of photoconversion in cells expressing mCamp2 WT (Fig. 3E).

A comparison of FACS-sorted photoactivated HEK293T cells found a significant difference in both the RFP/GFP ratio and the percentage PC between mCamp2 WT and mCamp2 Mutant transfected cells in the PC + No Agonist condition (Fig. 3F). Similarly, in HeLa cells, a significant difference was also observed in the percentage of photoconverted cells in the PC + No Agonist condition between mCamp2 WT and mCamp2 Mutant, while this difference was not observed in the RFP/GFP ratio metric (Fig. 3G). This discrepancy can be ascribed to the different aspects of the sample data described by the RFP/GFP ratio and percentage PC metrics. The RFP/GFP ratio only takes into account the average fluorescence values for the whole population of cells contained in the sample, making it sensitive to the magnitude of a Ca^{2+} mobilization but not to the number of cells which underwent a Ca^{2+}-dependent photoconversion. Conversely, the percentage PC metric only incorporates the influence of the number of

cells which underwent photoconversion, but disregards the magnitude of it. Percentage PC is also subject to variation based on the manual gating.

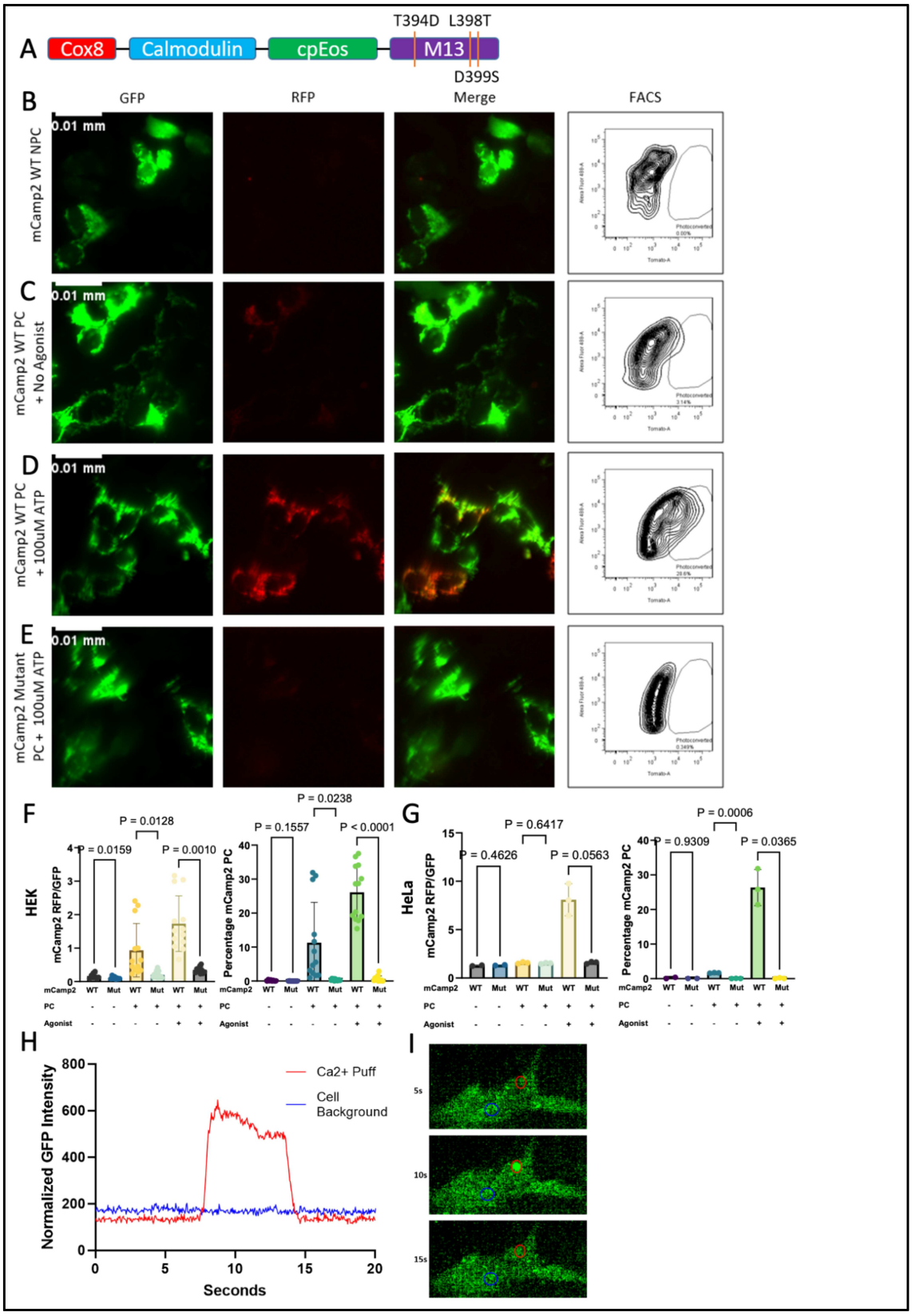

Figure 3. **The CaMPARI-FACS technique accurately measures Ca2+ and detects difficult to measure basal Ca2+ fluctuations. A.** Site directed mutagenesis on the M13 domain of mCamp2 generated a Ca^{2+}-insensitive mutant incapable of undergoing the conformational change required for green to red photoconversion after exposure to Ca^{2+} and PC light. **B.** mCamp2-transfected HEK293T cells in the NPC condition. From left to right GFP, RFP, and merged channels are shown under live cell imaging. GFP to RFP fluorescence plots obtained from FACS analysis are shown. **C.** mCamp2-transfected HEK293T cells in the PC + No Agonist condition. **D.** mCamp2-transfected HEK293T cells in the PC + 100uM ATP condition. **E.** mCamp2 Mutant-transfected HEK293T cells in the PC + 100uM ATP condition. **F**. CaMPARI-FACS results for mCamp2 WT and mCamp2 Mutant in HEK293T cells are shown with RFP/GFP ratio and Percentage PC metrics. A one-way ANOVA with Sidak's correction for multiple comparisons was performed on the groups exposed to the same condition. **G**. CaMPARI-FACS results for mCamp2 WT and mCamp2 Mutant in HeLa cells are shown with RFP/GFP ratio and Percentage PC metrics. A one-way ANOVA with Sidak's correction for multiple comparisons was performed on the groups exposed to the same condition. **H.** Polylysine-fixed HEK293WT cells stained with Fluo-4 and incubated with EGTA-AM were imaged with TIRF microscopy **I.** Representative image of cell In TIRF live cell imaging with ROIs corresponding to the traces in (**H**) circled in the relevant colors.

Regardless, these results indicate the existence of a correlation with the previously observed Ca^{2+} puffs in HEK 293T cells (13) and potentially HeLa cells. The presence of the Ca^{2+} puffs in the HEK293T cells was additionally confirmed with in-house measurements through TIRF microscopy. Basal, non-agonist evoked Ca^{2+} puffs were observed in one out of ten cells observed, indicating a low but extant incidence of this phenomenon in HEK293T cells. (Fig. 3H,I).

These results indicate that the photoactivation of mCamp2 is partially attributable to basal Ca^{2+} levels in and transfer to the mitochondria and not to the inherent fluorescent properties of the mCamp2 probe.

Overexpression of the IP3R1 does not modulate Ca^{2+} transfer across the MAMs

Previous studies demonstrating the modulability of mitochondrial Ca^{2+} dynamics (13) provided the target for testing the extent to which the photoconversion observed in the PC + No Agonist condition (Fig. 2E) is due to Ca^{2+}-related phenomena. It was previously reported that the three IP3R isoforms were the main actors in the transfer of Ca^{2+} from the ER to the mitochondria (9). Thus, overexpression of IP3R1 in HEK293T and HeLa cells would be expected to cause an increase of Ca^{2+} transfer to the mitochondria. On each cell line, live-cell imaging on cells dyed with Fura-2 and transfected with R-mito-Geco was compared to FACS on mCamp2-transfected photoactivated cells. In HEK 293T cells, live-cell imaging did not result in a visual difference in Ca^{2+} mobilization transients

between cells expressing a PCDNA3 control plasmid and cells expressing the IP3R1 plasmid (Fig. 4A). Conversely, HeLa cells displayed a visually discernible increase in amplitude of their cytosolic Ca^{2+} transients when transfected with IP3R1 compared to PCDNA3 (Fig. 4D). In both cell lines, there was no discernible change in the mitochondrial Ca^{2+} transients between PCDNA3 and IP3R1-transfected cells (Fig. 4B,E).

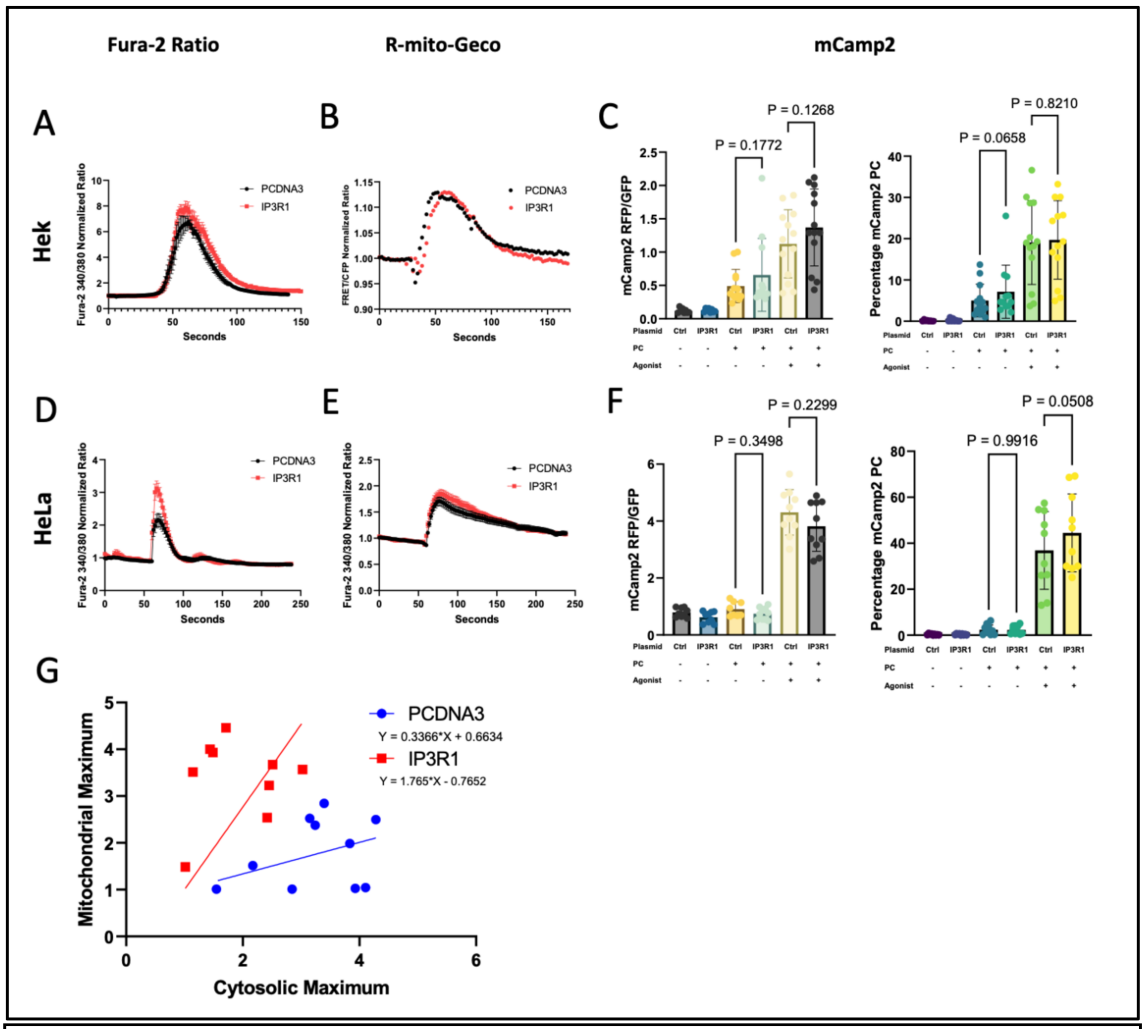

Figure 4. **Overexpression of IP3R1 does not lead to a measurable increase in Ca+ transfer to the mitochondria in HEK293T and HeLa cells. A.** Cytosolic Ca^{2+} change in response to 100 uM ATP was measured using Fura-2 in HEK293T. Traces represent an average of all responding cells with Standard Error of the Mean (SEM) error bars and were normalized to the first 20 seconds of the recording. **B**. Mitochondrial Ca^{2+} change was measured by cellularly expressed R-mito-Geco in HEK293T cells. **C.** HEK293T cells co-expressing mCamp2 and either PCDNA3 control plasmid or IP3R1 were photoconverted and measured for their RFP/GFP ratio and Percentage PC. An ANOVA mixed-effects analysis with a Geisser-Greenhouse correction was done for each cell line between the PCDNA3 and IP3R1 expressing cells for each condition. None of the differences were found to be significant (all p-values >0.0658). **D.** Cytosolic Ca^{2+} change in response to 50 uM Histamine was measured using Fura-2 in

HeLa. **E**. Mitochondrial Ca^{2+} change was measured by cellularly expressed R-mito-Geco in HeLa cells. **F.** HEK293T cells co-expressing mCamp2 and either PCDNA3 control plasmid or IP3R1 were photoconverted and measured for their RFP/GFP ratio and Percentage PC. An ANOVA mixed-effects analysis with a Geisser-Greenhouse correction was done for each cell line between the PCDNA3 and IP3R1 expressing cells for each condition. None of the differences were found to be significant (all p-values >0.0508). **F.** The Area Under the Curve (AUC) of the cytosolic and mitochondrial traces from (**A, B**) were compared for HeLa cells and simple linear regressions were used to visualize potential differences in cytosolic or mitochondrial Ca^{2+} dynamics between PCDNA3 control plasmid and IP3R1-transfected cells.

FACS of mCamp2-transfected photoactivated HEK293T and HeLa cells confirmed the results of the live-cell imaging of mitochondrial Ca^{2+}, without a significant difference in any of the PC + Agonist conditions between PCDNA3 and IP3R1-expressing cells (Fig. 4C,F). In both HEK and HeLa cells, there is a trend of increase in Ca^{2+} transfer between cells expressing PCDNA3 and cells expressing IP3R1 in both PC + No agonist and PC + Agonist conditions for FACS. However, none of the differences leading to this trend were found to be significant (all p-values >0.0508).

The presence of a weak trend in the FACS experiments together with the non-significant difference observed in the live cell imaging trials indicated that the experimental model was not ideal to represent a change in either basal or evoked mitochondrial Ca^{2+} transfer. The overexpression of IP3R1 may lead to an increase in basal and evoked mitochondrial Ca^{2+} transfer, but neither technique provides a clear answer to this question.

Reexpression of the IP3R1 in HEK293T IP3R Knock-out cells modulates both evoked and basal Ca^{2+} transfer across the MAMs

Given the fact that overexpression of IP3R1 did not provide an effective model for the modulation of mitochondrial Ca^{2+}, a proven model with a triple knockout for the three IP3R isoforms was used instead (HEK 3KO) (13). This cell line was shown to lack an evoked Ca^{2+} transfer response, which was partially rescuable with the reexpression of each of the individual isoforms (Fig. 5A). Using live-cell imaging with Fura-2 and the Ca^{2+}-mobilizing agonist Carbachol, HEK WT cells displayed a canonical agonist-induced cytosolic Ca^{2+} mobilization curve. Conversely, HEK 3KO cells display no cytosolic response to a Ca^{2+}-mobilizing agonist, consistently maintaining a flat trace. However, when the IP3R1 isoform is transiently reexpressed in a plasmid, the Ca^{2+}-mobilizing agonist elicits a cytosolic response, albeit a weaker one when compared to the HEK WT. (Fig. 5B,C) The same cells were also transfected with R-mito-GECO to observe the mitochondrial Ca^{2+} transfer transient, and a similar pattern was observed (Fig. 5D,E); HEK WT cells had a large predictable transient, HEK 3KO cells had no transient, while HEK 3KO + IP3R1 cells had a partially rescued Ca^{2+} transient.

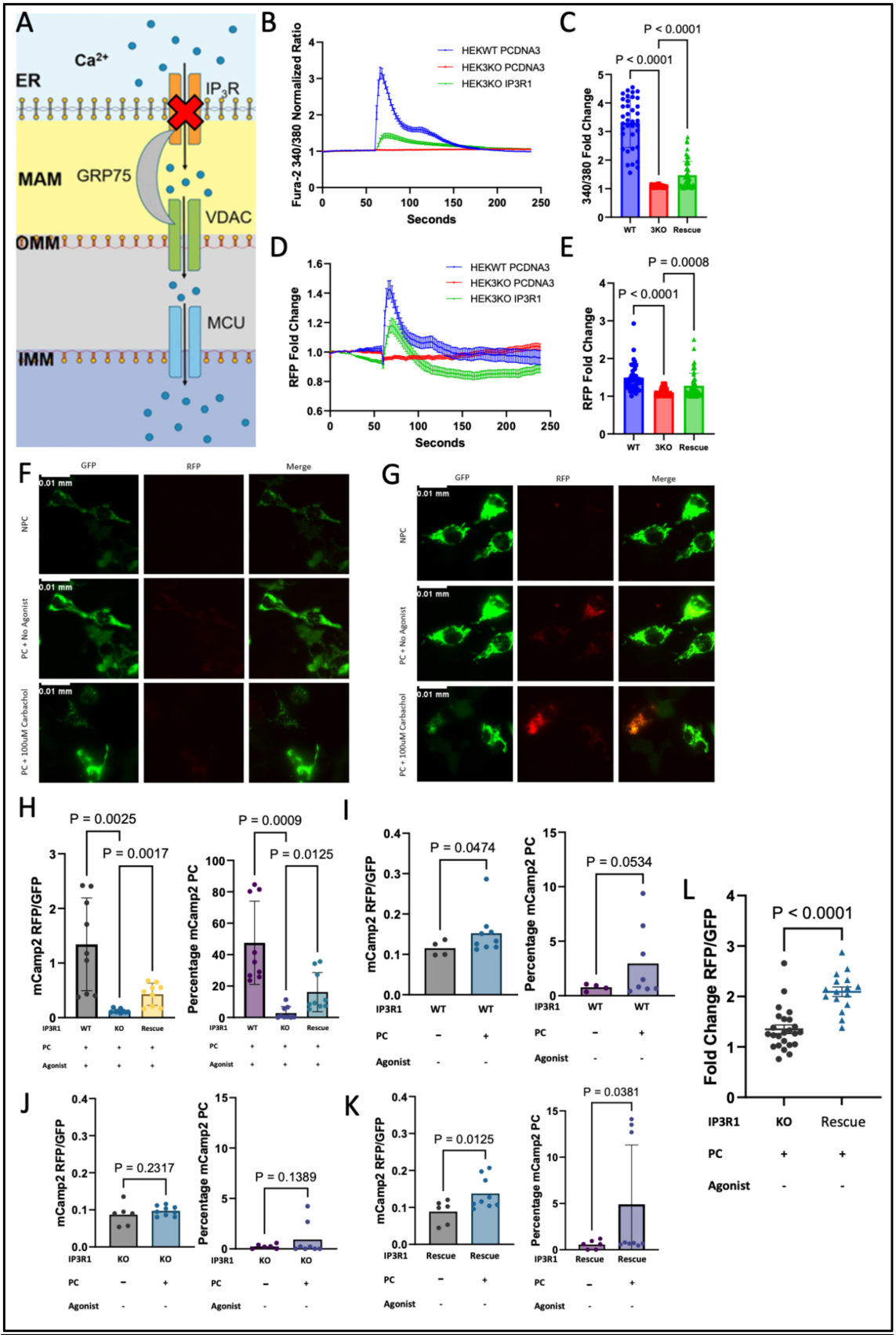

Figure 5. **IP3R1 re-expression partially rescues mitochondrial Ca^{2+} transfer in HEK293T IP3R 3KO cells. A.** Model for the HEK293T IP3R 3KO cells, showing

evoked mitochondrial Ca^{2+} transfer severely to entirely abrogated (image adapted from 29. Liu et al. 2021). **B.** Fura-2 staining was used to measure the evoked cytosolic Ca^{2+} change over time in HEK WT + PCDNA3 (blue), HEK 3KO + PCDNA3 (red), and HEK 3KO + IP3R1 (green) cells. 100uM Carbachol was used as a Ca^{2+}-mobilizing agonist. Traces represent an average of all cells expressing R-mito-GECO with error bars corresponding to SEM and were normalized to the first 20 seconds of the recording. **C.** Fold change of each cell model from the baseline to the transient maximum for Fura-2 traces. **D.** mCamp2-expressing HEK293T cells were photoconverted and analyzed for their RFP/GFP ratio and percentage PC using FACS. HEK WT cells were transfected with the PCDNA3 control plasmid while HEK 3KO cells were transfected either with the PCDNA3 control plasmid or IP3R1. Differences in evoked Ca^{2+} response between groups were tested using Brown-Forsythe and Welch ANOVA tests, with a significant difference found between the WT, the KO, and the rescue for the RFP/GFP ratio and between HEK WT and HEK 3KO for the percentage PC metric. **E.** Fold change of each cell model from the baseline to the transient maximum for R-mito-Geco traces. **F**. Live cell imaging of mCamp2 and PCDNA3-transfected HEK 3KO cells in NPC, PC + No Agonist, and PC + 100uM Carbachol conditions. For all three conditions, the RFP channel remained barely visible. **G.** Live cell imaging of mCamp2 and IP3R1-transfected HEK 3KO cells in NPC, PC + No Agonist, and PC + 100uM Carbachol conditions. The RFP channel becomes more visible in the PC + No Agonist and PC + 100uM Carbachol conditions. **H.** FACS of mCamp2-transfected cells in the PC + Agonist condition. **I**. HEK WT cells transfected with mCamp2 and PCDNA3 were analyzed by FACS in NPC and PC + No Agonist conditions. The difference between conditions was tested using Welch's one-tailed t-test and was found to be significant for the RFP/GFP Ratio (p= 0.0474). **J**. HEK 3KO cells transfected with mCamp2 and PCDNA3 were analyzed by FACS in NPC and PC + No Agonist conditions. The difference between conditions was tested using Welch's one-tailed t-test and was found to be not significant for the RFP/GFP Ratio (p= 0,2317). **K.** HEK 3KO cells transfected with mCamp2 and IP3R1 were analyzed by FACS in NPC and PC + No Agonist conditions. The difference between conditions was tested using Welch's one-tailed t-test and was found to be significant for the RFP/GFP Ratio (p= 0,0125) and the percentage photoconversion (p=0.0381). **L**. Graphical comparison between HEK 3KO and HEK 3KO + IP3R1 fluorescence intensity in live cell imaging. Fluorescence was normalized to background.

The same conditions were tested in cells which had been transfected with mCamp2 and subsequently measured with FACS, and a similar trend was observed in the PC + Agonist condition, with a significant difference observed between HEK WT, HEK 3KO, and HEK 3KO + IP3R1 cells (all p-values <0.0008), with the HEK 3KO + IP3R1 cells having an intermediate photoconversion between the HEK WT and HEK 3KO cells (Fig. 5H).

The results from the PC + Agonist condition were used as a control to understand the extent to which mCamp2 senses basal Ca^{2+} transfer to the mitochondria, The presence of Ca^{2+} transfer in the cell population was controlled for with the PC + Agonist condition, and only trials with a successful control were used for further analysis. The degree of photoconversion due to basal Ca^{2+} transfer was measured by comparing the mCamp2 RFP/GFP ratio and percentage PC for the NPC and PC + No Agonist conditions. If no significant difference between the NPC and PC + No Agonist conditions is observed in the HEK 3KO cells, that would indicate that the photoactivation of mCamp2 observed in the PC + No Agonist condition is entirely Ca^{2+} dependent and not due to other aspects of mCamp2.

While the HEK WT cells had a large statistically significant difference in mCamp2 photoconversion between the NPC and PC + No Agonist conditions for the RFP/GFP ratio (ratio p-value 0.0474; percentage PC p-value 0.0534) (Fig. 5I), the HEK 3KO cells exhibited no significant difference (ratio p-value 0.2317; percentage PC p-value 0.1389) (Fig. 5J). Expression of the IP3R1 in HEK 3KO cells partially rescued the phenotype of the HEK WT cells, restoring significance to the difference between the NPC and PC + No Agonist conditions (ratio p-value 0.0125; percentage PC p-value 0.0381) (Fig. 5K).

Expectedly, HEK 3KO cells transfected with mCamp2 and a PCDNA3 control plasmid had a visually less intense red fluorescence in PC + No Agonist and PC + Agonist conditions when compared to HEK 3KO cells transfected with mCamp2 and IP3R1 (Fig. 5F,G). The quantified relative RFP/GFP ratios from those images between the HEK 3KO cells expressing the PCDNA3 control plasmid and cells expressing the IP3R1 rescue plasmid were also found to be very significantly different ($p < 0.0001$) (Fig.5L).

Discussion

Utility of CaMPARI in Ca^{2+} Studies

With our research, we have demonstrated that CaMPARI is a useful tool for the effective and high-throughput measurement of subcellular Ca^{2+}. Like many other GECIs, CaMPARI already has several available variants with different subcellular localizations and Ca^{2+} binding affinities, making it highly adaptable. However, by using it in conjunction with FACS, we have been able to overcome some of the limitations faced by GECIs used with live-cell imaging: low-throughput experiments, qualitative analysis, and human bias in field of view selection.

By sacrificing the details of a Ca^{2+} transient normally obtained with live-cell imaging and focusing on two easily-interpretable metrics representing the integration of that transient over time, CaMPARI increases time efficiency of Ca^{2+} experiments. This means that CaMPARI does not answer the question ‘how does the Ca^{2+} transient look?’ but rather ‘is the Ca^{2+} concentration different between different conditions?’, which provides the advantage of being more quantifiable. CaMPARI’s use could easily be expanded to

screens aimed at identifying factors leading to Ca^{2+} perturbation. Similarly, if a Ca^{2+} perturbation is observed, CaMPARI could also be used to identify the contributing factors to that perturbation. For example, it is known that in some forms of ALS mitochondria experience a Ca^{2+} perturbation (31, 32), but the underlying cause of this has not been pinpointed; using CaMPARI, potential candidates could be screened for whether or not they cause a Ca^{2+} perturbation. The benefit of using the CaMPARI-FACS technique over traditional live-cell imaging in this situation is clear; for each Ca^{2+} perturbation candidate, CaMPARI-FACS collects data for thousands of cells in a matter of minutes while live-cell imaging requires hours to collect data for hundreds of cells.

When used to measure mitochondrial Ca^{2+}, mCamp2 is capable of measuring both the differences in spiking evoked by Ca^{2+} transfer from the ER, and the changes in basal Ca^{2+} in the mitochondria. Along with its high-throughput capabilities, it is clear that mCamp2 can be easily used as a tool for examining mitochondrial Ca^{2+} in the context of human disease. In addition, in this study, the MAMs were disrupted by overexpression and deletion of the IP3Rs, which had an effect on mitochondrial Ca^{2+}, which could be used as a concrete though indirect measure of MAMs perturbation. As MAMs are an important signaling hub in many cellular signaling pathways, CaMPARI opens the potential to using mitochondrial Ca^{2+} levels as an indicator for cellular homeostasis disruptions.

Basal Ca^{2+} Transfer

As we have seen in this study, basal mitochondrial Ca^{2+} was changed by knockout then rescue of the IP3R1; the nature of this basal mitochondrial Ca^{2+}, however, is still unclear. The potential exists for this basal mitochondrial Ca^{2+} dependence of IP3Rs to be a static maintenance between evoked Ca^{2+} transfer events. Alternatively, the non-evoked Ca^{2+} puffs observed in this study and by Lock et al. (13) could also contribute to basal mitochondrial Ca^{2+} levels. The significance of these Ca^{2+} puffs has yet to be explained and could be an interesting novel feature of IP3Rs.

Additionally, the IP3R1 isoform when reexpressed only partially rescues both basal and evoked Ca^{2+} transfer, indicating an important role for the IP3R2 and IP3R3 isoforms. Exploration of this would provide the opportunity to further understand the functional differences between the three isoforms. The fact remains that removal of all three IP3R practically eliminates the differences between basal and evoked Ca^{2+} transfer levels also supports the theory that the entry of Ca^{2+} into the mitochondria is likely exclusively modulated by MAMs and not possible directly from the cytosol (8).

Finally, the influence of IP3R1 overexpression was left unclear. Though the presence of a trend in increasing evoked and basal mitochondrial Ca^{2+} indicated some modulation, the trend was very weak and not statistically significant. Further investigation with complementation by other more precise techniques would be required to answer this question.

Limitations of the study

The largest barrier to the accurate measurement of Ca^{2+} using the CaMPARI-FACS technique is the high variability in the photoconversion of mCamp2 between different days. There was always consistency between FACS tubes of the same condition on the same day, but we observed that factors such as cell confluency, passage number, and level of ambient light in the room when the experiment was performed affected the magnitude of photoconversion, especially in the PC + agonist conditions. These results led us to believe that the cells' responsiveness to an agonist was highly dependent on the culture conditions prior to and during the photoconversion experiment. Additionally, the contribution of dead cells to Ca^{2+}-mediated mCamp2 photoconversion was left unexplored, as we decided to exclude dead cells from our FACS experiments by Sytox Blue staining and from live cell imaging experiments with visual inspection of fluorescence pattern, a diffuse fluorescence pattern indicating a dead or dying cell.

Methods

Cell Culture

Hek293 and HEK293 IP3R triple knockout cells were kept in Dulbecco's Modified Eagle's Medium (DMEM) medium with 10% Fetal Calf Serum (FCS) and 1% Penstrep (PS). HEK293 3KO cells were obtained from the laboratory of David Yule (13). NSC34 cells were maintained in DMEM with 4.5g/L glucose, 1% MEM NEAA, 1% PS, and 10% FCS. Low glucose conditions for these cells were adjusted to DMEM with 1g/L glucose, 1% MEM Non-Essential Amino Acids (NEAA), 1% PS, and 10% FCS, where the cells were kept for 5 days prior to experiments. Transfection was carried out using Lipofectamine in DMEM base media with 1ug of plasmid per 35mm plate. HeLa cells were maintained in Eagle's Minimum Essential Medium (EMEM) with 1g/L glucose, 1% MEM NEAA, 1% PS, and 10% FCS.

mCamp2 Photoconversion

Cells 48 hours post-transfection with mCamp2 and additional plasmids were seeded in 24 or 48-well plates. The culture medium was replaced with 2mM Ca^{2+}-containing medium (140 mM NaCl, 5 mM KCl, 1 mM MgCl2, 2 mM CaCl2, 20 mM Hepes, 10 mM glucose, adjusted to pH 7.4, with NaOH), and the plate was placed under an LED lamp emitting 365nm, 385nm, and 405 nm light (180 seconds LED power; 20mW/cm2) (30). Upon activation of the light, chemical agonists for MAMs Ca^{2+} transfer were added in 2mM Ca^{2+} solution. For HEK293 cells and derivatives, the agonists used were 50uM Na+-ATP, the IP3-specific agonist IP3AM at 50uM; and Carbachol (CCH) at 100uM. For HeLa cells, MAMs Ca^{2+} transfer was elicited using 100uM histamine. In NSC34 cells, 50uM ATP was used. Cells were left under the photoconverting light for 3 minutes after addition of the agonist, after which time, the agonist-containing medium was aspirated and cells were incubated in Trypsin containing 2uM Sytox blue cell death marker until detachment, at which point they were resuspended and transferred to culture-medium containing flow cytometry tubes on ice.

Fluorescence-activated cell sorting

A BD LSR Fortessa Cell Analyzer was used to sort cells. Cells were sorted first by shape (FCS-A), multiplicity (SSC-A), Sytox blue staining, and mCamp2 transfection. Only living cells negative for Sytox blue and with a 10^3 level of mCamp2 green fluorescence were selected for analysis. Gating for photoconversion was normalized using a non-photoconverted (NPC) control. Analysis was completed using FlowJo software and photoconversion was determined by percentage passing threshold established by NPC control as well as RFP/GFP signal ratio per population. Charts illustrating data were created using GraphPad Prism.

Live-cell Imaging

Live cell imaging was performed on a Leica SP5 2P microscope controlled by Leica Application Suite software (Leica AG, Germany) in 35mm chambers. Cells were seeded on 25mm coverslips 24 hours before the experiment after transfection with R-mito-Geco (addgene: 46021) and other desired plasmids. Coverslips were incubated in 2uM Fura-2 in 2mM Ca^{2+} solution for 25 minutes. Cells were washed for 5 minutes with 2mM Ca^{2+} solution then placed on the microscope. Fields of view were selected based on the optimal number of cells transfected with sensors of interest being present. Recording was carried out in 2 second intervals. 30 intervals were allowed to pass before addition of the agonist, and the recording was continued for a total of 120 time points. Three channels were used for the duration of the recording: 340 Fura-2 (ex 340 em 510 +/-20); 380 Fura-2 (ex 380 em 510 +/20); and mCherry (ex 550 em 610+/- 40). Images were analyzed using ImageJ. Fura traces were generated using a ratio of 340/380 normalized to the average of the first 10 timepoints with a subtracted background. R-mito-Geco traces were also normalized to the average of the first 10 timepoints with a subtracted background. Graphs were generated using GraphPad Prism.

TIRF Microscopy

Cells were seeded on 25mm coverslips coated with polylysine 24 hours before imaging. Before imaging, cells were incubated for 1 hour in 5uM fluo-4, then 45 minutes in 2,5uM Sytox Blue, 5uM EGTA-AM, and 1:5000 cell mask, and were left in 2mM Ca^{2+}-containing medium. Cells were imaged for 30 seconds at 50 ms time points. Imaging was performed using a Nikon Eclipse Ti microscope equipped with a Perfect Focus System (PFS III) using a 100× oil CFI Apochromat TIRF Objective (NA 1.49; Nikon Instruments Europe B.V.).

Bibliography

1. Giorgi C, Missiroli S, Patergnani S, Duszynski J, Wieckowski MR, Pinton P. Mitochondria-associated membranes: composition, molecular mechanisms, and physiopathological implications. Antioxid Redox Signal. 2015 Apr 20;22(12):995-1019. doi: 10.1089/ars.2014.6223. Epub 2015 Mar 13. PMID: 25557408.

2. van Vliet AR, Verfaillie T, Agostinis P. New functions of mitochondria associated membranes in cellular signaling. Biochim Biophys Acta. 2014 Oct;1843(10):2253-62. doi: 10.1016/j.bbamcr.2014.03.009. Epub 2014 Mar 15. PMID: 24642268.
3. Pinton, P., Giorgi, C., Siviero, R. et al. Calcium and apoptosis: ER-mitochondria Ca2+ transfer in the control of apoptosis. Oncogene 27, 6407–6418 (2008). https://doi.org/10.1038/onc.2008.308
4. Rosario Rizzuto et al., Close Contacts with the Endoplasmic Reticulum as Determinants of Mitochondrial Ca2+ Responses. Science 280, 1763-1766(1998). DOI: 10.1126/science.280.5370.1763
5. Csordás G, Weaver D, Hajnóczky G. Endoplasmic Reticulum-Mitochondrial Contactology: Structure and Signaling Functions. Trends Cell Biol. 2018 Jul;28(7):523-540. doi: 10.1016/j.tcb.2018.02.009. Epub 2018 Mar 24. PMID: 29588129; PMCID: PMC6005738.
6. Lewis RS. Store-operated calcium channels: new perspectives on mechanism and function. Cold Spring Harb Perspect Biol. 2011 Dec 1;3(12):a003970. doi: 10.1101/cshperspect.a003970. PMID: 21791698; PMCID: PMC3225942.
7. Phillips, M., Voeltz, G. Structure and function of ER membrane contact sites with other organelles. Nat Rev Mol Cell Biol 17, 69–82 (2016). https://doi.org/10.1038/nrm.2015.8
8. Jouaville LS, Pinton P, Bastianutto C, Rutter GA, Rizzuto R. Regulation of mitochondrial ATP synthesis by calcium: evidence for a long-term metabolic priming. Proc Natl Acad Sci U S A. 1999 Nov 23;96(24):13807-12. doi: 10.1073/pnas.96.24.13807. PMID: 10570154; PMCID: PMC24146.
9. Rizzuto R, Marchi S, Bonora M, Aguiari P, Bononi A, De Stefani D, Giorgi C, Leo S, Rimessi A, Siviero R, Zecchini E, Pinton P. Ca(2+) transfer from the ER to mitochondria: when, how and why. Biochim Biophys Acta. 2009 Nov;1787(11):1342-51. doi: 10.1016/j.bbabio.2009.03.015. Epub 2009 Mar 31. PMID: 19341702; PMCID: PMC2730423.
10. Prole DL, Taylor CW. Structure and Function of IP3 Receptors. Cold Spring Harb Perspect Biol. 2019 Apr 1;11(4):a035063. doi: 10.1101/cshperspect.a035063. PMID: 30745293; PMCID: PMC6442203.
11. Rosencrans WM, Rajendran M, Bezrukov SM, Rostovtseva TK. VDAC regulation of mitochondrial calcium flux: From channel biophysics to disease. Cell Calcium. 2021 Mar;94:102356. doi: 10.1016/j.ceca.2021.102356. Epub 2021 Jan 23. PMID: 33529977; PMCID: PMC7914209.
12. De Stefani D, Raffaello A, Teardo E, Szabò I, Rizzuto R. A forty-kilodalton protein of the inner membrane is the mitochondrial calcium uniporter. Nature. 2011 Jun 19;476(7360):336-40. doi: 10.1038/nature10230. PMID: 21685888; PMCID: PMC4141877.
13. Lock JT, Alzayady KJ, Yule DI, Parker I. All three IP3 receptor isoforms generate Ca2+ puffs that display similar characteristics. Sci Signal. 2018 Dec

18;11(561):eaau0344. doi: 10.1126/scisignal.aau0344. PMID: 30563861; PMCID: PMC6402561.
14. Fish KN. Total internal reflection fluorescence (TIRF) microscopy. Curr Protoc Cytom. 2009 Oct;Chapter 12:Unit12.18. doi: 10.1002/0471142956.cy1218s50. PMID: 19816922; PMCID: PMC4540339.
15. Giorgi C, Marchi S, Pinton P. The machineries, regulation and cellular functions of mitochondrial calcium. Nat Rev Mol Cell Biol. 2018 Nov;19(11):713-730. doi: 10.1038/s41580-018-0052-8. Erratum in: Nat Rev Mol Cell Biol. 2018 Sep 24;: PMID: 30143745.
16. Tarasov AI, Griffiths EJ, Rutter GA. Regulation of ATP production by mitochondrial Ca(2+). Cell Calcium. 2012 Jul;52(1):28-35. doi: 10.1016/j.ceca.2012.03.003. Epub 2012 Apr 12. PMID: 22502861; PMCID: PMC3396849.
17. Marcu R, Wiczer BM, Neeley CK, Hawkins BJ. Mitochondrial matrix Ca^{2+} accumulation regulates cytosolic NAD^{+}/NADH metabolism, protein acetylation, and sirtuin expression. Mol Cell Biol. 2014 Aug;34(15):2890-902. doi: 10.1128/MCB.00068-14. Epub 2014 May 27. PMID: 24865966; PMCID: PMC4135570.
18. Cárdenas C, Miller RA, Smith I, Bui T, Molgó J, Müller M, Vais H, Cheung KH, Yang J, Parker I, Thompson CB, Birnbaum MJ, Hallows KR, Foskett JK. Essential regulation of cell bioenergetics by constitutive InsP3 receptor Ca2+ transfer to mitochondria. Cell. 2010 Jul 23;142(2):270-83. doi: 10.1016/j.cell.2010.06.007. PMID: 20655468; PMCID: PMC2911450.
19. T.M. Bauer, E. Murphy. Role of mitochondrial calcium and the permeability transition pore in regulating cell death. Circ. Res., 126 (2020), pp. 280-293, 10.1161/CIRCRESAHA.119.316306.
20. Pinton, P. Mitochondria-associated membranes (MAMs) and pathologies. Cell Death Dis 9, 413 (2018). https://doi.org/10.1038/s41419-018-0424-1.
21. Kerkhofs, M., Bittremieux, M., Morciano, G. et al. Emerging molecular mechanisms in chemotherapy: Ca2+ signaling at the mitochondria-associated endoplasmic reticulum membranes. Cell Death Dis 9, 334 (2018). https://doi.org/10.1038/s41419-017-0179-0.
22. Kurt J. De Vos and others, VAPB interacts with the mitochondrial protein PTPIP51 to regulate calcium homeostasis, Human Molecular Genetics, Volume 21, Issue 6, 15 March 2012, Pages 1299–1311, https://doi.org/10.1093/hmg/ddr559.
23. Le Gall L, Anakor E, Connolly O, Vijayakumar UG, Duddy WJ, Duguez S. Molecular and Cellular Mechanisms Affected in ALS. J Pers Med. 2020 Aug 25;10(3):101. doi: 10.3390/jpm10030101. PMID: 32854276; PMCID: PMC7564998.
24. Bagur R, Hajnóczky G. Intracellular Ca2+ Sensing: Its Role in Calcium Homeostasis and Signaling. Mol Cell. 2017 Jun 15;66(6):780-788. doi: 10.1016/j.molcel.2017.05.028. PMID: 28622523; PMCID: PMC5657234.

25. Wu J, Liu L, Matsuda T, Zhao Y, Rebane A, Drobizhev M, Chang YF, Araki S, Arai Y, March K, Hughes TE, Sagou K, Miyata T, Nagai T, Li WH, Campbell RE. Improved orange and red Ca²± indicators and photophysical considerations for optogenetic applications. ACS Chem Neurosci. 2013 Jun 19;4(6):963-72. doi: 10.1021/cn400012b. Epub 2013 Mar 19. PMID: 23452507; PMCID: PMC3689190.
26. Jensen, E.C. (2013), Overview of Live-Cell Imaging: Requirements and Methods Used. Anat Rec, 296: 1-8. https://doi.org/10.1002/ar.22554.
27. Benjamin F. Fosque et al., ,Labeling of active neural circuits in vivo with designed calcium integrators.Science347,755-760(2015).DOI:10.1126/science.1260922.
28. Hoi H, Matsuda T, Nagai T, Campbell RE. Highlightable Ca2+ indicators for live cell imaging. J Am Chem Soc. 2013 Jan 9;135(1):46-9. doi: 10.1021/ja310184a. Epub 2012 Dec 26. PMID: 23256581.
29. Jinxuan Liu, Jinghua Yang, Mitochondria-associated membranes: A hub for neurodegenerative diseases, Biomedicine & Pharmacotherapy, Volume 149, 2022, 112890, ISSN 0753-3322, https://doi.org/10.1016/j.biopha.2022.112890.
30. Amado Carreras-Sureda, Laurence Abrami, Kim Ji-Hee, Wen-An Wang, Christopher Henry, Maud Frieden, Monica Didier, F Gisou van der Goot, Nicolas Demaurex (2021) S-acylation by ZDHHC20 targets ORAI1 channels to lipid rafts for efficient Ca2+ signaling by Jurkat T cell receptors at the immune synapse eLife 10:e72051
31. Stoica R, De Vos KJ, Paillusson S, Mueller S, Sancho RM, Lau KF, Vizcay-Barrena G, Lin WL, Xu YF, Lewis J, Dickson DW, Petrucelli L, Mitchell JC, Shaw CE, Miller CC. ER-mitochondria associations are regulated by the VAPB-PTPIP51 interaction and are disrupted by ALS/FTD-associated TDP-43. Nat Commun. 2014 Jun 3;5:3996. doi: 10.1038/ncomms4996. PMID: 24893131; PMCID: PMC4046113.
32. Stoica R, De Vos KJ, Paillusson S, Mueller S, Sancho RM, Lau KF, Vizcay-Barrena G, Lin WL, Xu YF, Lewis J, Dickson DW, Petrucelli L, Mitchell JC, Shaw CE, Miller CC. ER-mitochondria associations are regulated by the VAPB-PTPIP51 interaction and are disrupted by ALS/FTD-associated TDP-43. Nat Commun. 2014 Jun 3;5:3996. doi: 10.1038/ncomms4996. PMID: 24893131; PMCID: PMC4046113.